Acta Crystallographica Section B
Structural Science
ISSN 0108-7681

Intergrowth polytypoids as modulated structures: a superspace description of the $Sr_n(Nb,Ti)_nO_{3n+2}$ compound series

L. Elcoro,[a]* J. M. Perez-Mato[a] and R. L. Withers[b]

[a]Departamento de Física de la Materia Condensada, Facultad de Ciencias, Universidad del Pais Vasco, Apdo 644, E-48080 Bilbao, Spain, and [b]Research School of Chemistry, Australian National University, Canberra, ACT 0200, Australia

Correspondence e-mail: wmpelcel@lg.ehu.es

Received 24 January 2001
Accepted 28 March 2001

A new, unified superspace approach to the structural characterization of the perovskite-related $Sr_n(Nb,Ti)_nO_{3n+2}$ compound series, strontium niobium/titanium oxide, is presented. To a first approximation, the structure of any member of this compound series can be described in terms of the stacking of (110)-bounded perovskite slabs, the number of atomic layers in a single perovskite slab varying systematically with composition. The various composition-dependent layer-stacking sequences can be interpreted in terms of the structural modulation of a common underlying average structure. The average interlayer separation distance is directly related to the average structure periodicity along the layer stacking direction, while an inherent modulation thereof is produced by the presence of different types of layers (particularly vacant layers) along this stacking direction. The fundamental atomic modulation is therefore occupational and can be described by means of crenel (step-like) functions which define occupational atomic domains in the superspace, similarly to what occurs for quasicrystals. While in a standard crystallographic approach, one must describe each structure (in particular the space group and cell parameters) separately for each composition, the proposed superspace model is essentially common to the whole compound series. The superspace symmetry group is unique, while the primary modulation wavevector and the width of some occupation domains vary linearly with composition. For each rational composition, the corresponding conventional three-dimensional space group can be derived from the common superspace group. The resultant possible three-dimensional space groups are in agreement with all the symmetries reported for members of the series. The symmetry-breaking phase transitions with temperature observed in many compounds can be explained in terms of a change in superspace group, again in common for the whole compound series. Inclusion of the incommensurate phases, present in many compounds of the series, lifts the analysis into a five-dimensional superspace. The various four-dimensional superspace groups reported for this incommensurate phase at different compositions are shown to be predictable from a proposed five-dimensional superspace group apparently common to the whole compound series. A comparison with the scarce number of refined structures in this system and the homologous $(Nb,Ca)_6Ti_6O_{20}$ compound demonstrates the suitability of the proposed formalism.

1. Introduction

One of the most important characteristics of perovskite-related structures is their compositional flexibility. This

compositional flexibility arises from the ability of the perovskite structure-type (ABX_3 ideal composition) to regularly intergrow with layers of alternate local structure-type. Well known examples include Aurivillius (Aurivillius, 1949, 1950) and Ruddlesden–Popper (Ruddlesden & Popper, 1958) type phases, whereby perovskite blocks regularly intergrow with Bi_2O_2 and NaCl-like layers, respectively. Both these examples involve intergrowth along an ideal $\langle 100\rangle_p$ direction (in the following the subscript p represents the cubic basis of the ideal perovskite structure-type). Intergrowth along a $\langle 100\rangle_p$ direction, however, is not the only intergrowth direction possible. B-deficient compounds, $A_nB_{n-\delta}X_{3n}$ or $AB_{1-x}X_3$, for example, can be formed by the intergrowth of $\langle 111\rangle_p$ cubic perovskite-type slabs with B-deficient hexagonal close packed layers. Such structures are most easily described in terms of the alternate stacking of AX_3 and B layers along the $\langle 111\rangle_p$ direction of an ideal perovskite-type structure. The vacancies occur as entire B layers and there are x vacant layers for each AX_3 layer (Van Tendeloo *et al.*, 1994).

Initially, superspace crystallography was introduced in the late seventies by de Wolff, Janner and Janssen (Janssen *et al.*, 1992) to deal with the quantitative analysis of incommensurately modulated phases with temperature-dependent modulation wavevectors. Soon, however, this approach was generalized to more general non-periodic phases such as incommensurate composite structures and quasicrystals (Janner & Janssen, 1980; Bak, 1985, 1986). The main point of the formalism is the unique indexation of the diffraction pattern with a basis of $3 + d$ vectors. Fourier transform properties relating projections and sections in direct and reciprocal spaces allow the real three-dimensional physical structure to be interpreted as a section of a periodic $(3 + d)$-dimensional structure. The complementary d-dimensional subspace is called internal space. The rotational symmetry and systematic extinctions of the diffraction pattern permit the assignation of a $(3 + d)$-dimensional superspace group. Structure determination is thus now carried out in $(3 + d)$ dimensions, where the periodicity combined with the known superspace-group symmetry simplifies matters considerably. Atoms are described in superspace as d-dimensional objects called atomic surfaces or atomic domains (in the following AS). A section through such an atomic surface gives rise to a single point where the atom is located in the real physical structure. For incommensurately modulated structures and composites, the AS's are usually described by means of continuous functions along the whole internal space, while for quasicrystals the atomic domains have finite boundaries. The superspace approach can be easily extended to commensurate structures, where it is very useful for efficiently describing and analyzing atomic correlations which lie outside the conventional space-group symmetry relations (Perez-Mato, 1992; Withers *et al.*, 1998). Intergrowth layer compounds and polytypoids (Verma & Trigunayat, 1974; Rao & Rao, 1978; Krishna, 1983) are also suitable for such a description because they are built up by the stacking of a finite set of independent atomic layers. The number of layers per unit cell can be large, so that the atoms within the unit cell exhibit approximate average periodicities of a smaller length scale than the unit-cell parameters. The occupational domains are step-like (crenel) functions which represent the different types of layers in the stacking sequences and the modulation wavevector magnitude depends on the relative amounts of those layers. In such systems, structure cannot be interpreted in terms of a small modulation of an average structure due to the discontinuity of the AS's.

These ideas have already been successfully applied to the structure determination of $A_{1+x}BO_3$-type compounds (Evain *et al.*, 1998; Perez-Mato *et al.*, 1999; Gourdon *et al.*, 2000) and, in a recent paper, we reported an analysis of the compound series $La_nTi_{n-\delta}O_{3n}$ in this superspace framework. A single superspace model was found to be sufficient to reproduce the observed structures over the whole range of composition. The only variable parameters required to move from one composition to another were the size of the AS's which describe the atoms in superspace and the associated primary modulation wavevector, while the superspace group remained invariant. The AS's turned out to be well described by means of crenel occupational functions along internal space in conjunction with sawtooth-shaped displacive modulations along the stacking direction (Elcoro *et al.*, 2000).

In the present paper we apply a superspace construction to the description of another compositionally flexible perovskite-related compound series with stoichiometry $A_nB_nX_{3n+2}$. Such structures can be interpreted in terms of the stacking of layers of octahedra along a $\langle 110\rangle_p$ direction of the ideal perovskite structure. This compound series has recently been studied by Levin and co-workers (Levin & Bendersky, 1999), who presented a general review of conventional symmetry properties and transmision electron microscopy results for A = Sr, B = Nb, Ti and X = O (Levin *et al.*, 1998, 2000). They provided experimental results for compounds corresponding to the integer values $n = 4, 5, 6, 7$, as well as the rational value $n = 4.5$. The minimum value in this particular system, $n = 4$, is fixed by valence considerations. In addition, the authors summarized the published structure determinations of some $A_nB_nX_{3n+2}$-type structures (see Table 1 in Levin & Bendersky, 1999).

In all compounds of the series, when experimental conditions have permitted analysis up until the melting point, the following sequence of phase transitions has been found as temperature is lowered:

$$\text{untilted orthorhombic} \longrightarrow \text{tilted orthorhombic} \longrightarrow \text{incommensurate} \longrightarrow \text{monoclinic},$$

where tilted indicates a small correlated rotation of octahedra around the **a** axis of the ideal perovskite structure. A limited range of accessibility has, however, sometimes not permitted the observation of all these potential phase transitions (at high temperature in some cases or at low temperature in other cases). For all compositions, the incommensurate primary modulation wavevector has been found to be parallel to the **a*** axis with a magnitude close to 0.5.

The conventional space-group symmetries of the tilted and untilted orthorhombic phases for the $n = 4, 5, 6, 7$ members of

Table 1
Sequences of phase transitions with temperature for several members of the $Sr_n(Nb, Ti)_nO_{3n+2}$ compound series and isomorphous compounds.

Compound	Untilted orthogonal⟶ tilted orthogonal ⟶ incommensurate ⟶ monoclinic
$Sr_2Nb_2O_7$ ($n = 4$)$^{(a,b)}$	$Cmcm \xrightarrow{1643\ K} Cmc2_1 \xrightarrow{488\ K} Cmc2_1(\gamma'00)0s0 >$ at least 103 K
$Sr_5TiNb_4O_{17}$ ($n = 5$)$^{(b)}$	$Immm \xrightarrow{873\ K} Pmnn \xrightarrow{523\ K} Pmnn(\gamma'00)000 \xrightarrow{453\ K} P112_1/b$
$Sr_6Ti_2Nb_4O_{20}$ ($n = 6$)$^{(b)}$	$Cmcm \longrightarrow Cmc2_1 \xrightarrow{473\ K} Cmc2_1(\gamma'00)0s0 >$ at least 103 K
$Sr_7Ti_3Nb_4O_{23}$ ($n = 7$)$^{(b)}$	$Immm \xrightarrow{743\ K} Pmnn \xrightarrow{373\ K} Pmnn(\gamma'00)000 >$ at least 103 K
$La_2Ti_2O_7$ ($n = 4$)$^{(c)}$	$Cmcm \xrightarrow{1773\ K} Cmc2_1 \xrightarrow{1053\ K} Cmc2_1(\gamma'00)0s0 \xrightarrow{993\ K} P112_1$
$Nd_4Ca_2Ti_6O_{20}$ ($n = 6$)$^{(d,e)}$	at least 1623 K > $Cmc2_1(\gamma'00)0s0$
$Sr_{4.5}Ti_{0.5}Nb_4O_{15.5}$ ($n = 4.5$)$^{(b)}$	at least 1273 K > $Pmcb \longrightarrow P112_1/b$

References: (*a*) Yamamoto (1982), (*b*) Levin *et al.* (2000), (*c*) Tanaka *et al.* (1985), (*d*) Grebille & Berar (1987), (*e*) Nanot *et al.* (1986).

the $Sr_n(Nb, Ti)_nO_{3n+2}$ series and other related phases are summarized in Table 1. The incommensurate phase has not been observed for the $n = 4.5$ compound, while the transition from the tilted orthorhombic to the monoclinic phase seems to be direct in this case. Both the space-group symmetries and the transition temperatures depend on composition. In a standard crystallographic description, one must analyze separately the structure and the sequence of phase transitions for each member of the series. The approximate layered structure of the compounds suggests the application of the superspace approach to this system. This is supported by the continuously variable, composition-dependent character of the published diffraction patterns, where the existence of a unique average structure for all compositions can be inferred from the common set of strong reflections.

The paper is organized as follows: in the next section the main features of the structures are described, introducing the required notation for the stacking layers. The third section is devoted to the superspace description of the high-temperature untilted phase, tilted phases at intermediate temperatures and incommensurate phases. The relevant superspace groups are determined from the published diffraction patterns (Levin *et al.*, 2000) as well as the resulting possible space groups for any composition. Symmetry restrictions on the AS's and the additional symmetry-allowed displacive degrees of freedom which are necessary to improve the superspace description are then determined. Finally, in the fourth section the structural data available up to now for some members of the series is then compared with the proposed model, showing the form of the displacive modulations associated with the crenel functions, and confirming the validity of the approach.

2. The layer model

According to Levin *et al.* (2000), to a first approximation, the structure of the compounds $Sr_n(Nb, Ti)_nO_{3n+2}$ at any composition (n can have non-integral values) is orthorhombic and consists of slabs of $(Ti, Nb)O_6$ octahedra (the width of which is composition-dependent), stacked along the $[011]_p$ direction of the ideal cubic perovskite structure. This stacking direction is conventionally labeled the **b** axis. As the width of these perovskite slabs or the number of layers in a period varies for different values of n, the magnitude of the lattice parameter b is necessarily composition-dependent. The other two orthogonal unit-cell vectors, $\mathbf{a} = [100]_p$ and $\mathbf{c} = [0\bar{1}1]_p$ span the $(011)_p$ layers of octahedra and are practically composition independent ($a \simeq a_p = 3.933$ Å, $c \simeq 2^{1/2}\mathbf{a}_p \simeq 5.562$ Å). Figs. 1(*a*) and (*b*) show the layer stacking sequence for the $n = 4$ member. For any integer n, the unit cell along the **b** direction contains two slabs of n octahedral layers. In the limit case $n = \infty$ there is a single infinite slab which corresponds to the ideal perovskite structure. Sr atoms are located in the center of a rectangle of four (Ti,Nb) atoms, which are the centers of four octahedra within these $(011)_p$ layers. In a standard crystallographic approach, this interpretation of the structure in terms of octahedral units has advantages. Firstly, the structure at intermediate temperatures can be described in terms of a slight distortion away from ideal perovskite stacking. The practically rigid octahedra are tilted only a small amount around one of the crystallographic axes (the **a** axis). On the other hand, the rest of the displacive phase transitions present for all integer compositions can be described by extra tilts of these octahedral units (Levin & Bendersky, 1999; Levin *et al.*, 2000).

Alternatively, rather than octahedral layers, the structure can be described in terms of the stacking of individual atomic layers. This viewpoint is more suitable for a superspace analysis. Along any $\langle 110\rangle_p$ direction, the ideal perovskite structure (the $n = \infty$ member of the compound series, usually considered as a reference structure) consists of the alternate stacking of Sr(Ti,Nb)O and O_2 individual atomic layers. The oxygen positions within the O_2 layers (denoted by the symbol O in the following) are given by $(x, z) = \left(\frac{1}{2}, \frac{1}{4}\right)$ and $\left(\frac{1}{2}, \frac{3}{4}\right)$, respectively, as shown in Fig. 1(*c*). Unlike for the O-type layers, there are two types of Sr(Ti,Nb)O layers, which will be denoted by the symbols M and N. The atomic positions in the M-type layer are given by $(x, z) = (0, 0)$, $\left(\frac{1}{2}, \frac{1}{2}\right)$ and $\left(0, \frac{1}{2}\right)$, for Sr, (Ti/Nb) and O atoms, respectively, as shown in Fig. 1(*d*). The corresponding positions in the N-type layer are shifted $\frac{1}{2}$ along the **c** direction with respect to those of the M-type layer. The complete set of atomic layers in a single period of the perfect ideal perovskite structure is thus MONO. Each of the M or N layers are sandwiched between two O layers, so that each Nb/Ti atom is surrounded by six O atoms: two in the same layer, and two in each of the surrounding O layers, thus forming an octahedron. A single $(011)_p$ layer of octahedra is thus formed by the three consecutive atomic layers OMO or

ONO. From one such octahedral layer to the next, the octahedra are shifted $\frac{1}{2}$ along the **c** axis, so that consecutive octahedra share corners (see Figs. 1*a* and *b*). For a general composition $Sr_n(Nb, Ti)_nO_{3n+2}$, the extra oxygen atoms occur as entire additional O layers. The overall composition requires that, for each *n* (MO/NO) pairs, one extra O atomic layer must be accommodated next to another O layer without an intermediate M or N layer. Thus, consecutive OO layers will appear in the stacking sequence. An alternative but equivalent viewpoint is that there is a vacant M or N layer on average for each (*n* + 1) MO/NO sequence. For instance, two periods of the *n* = 4 sequence can be written, OMONOMONO∅OMONOMONO∅, where the symbol ∅ represents a vacant M or N layer. The two octahedra on either side of the vacant layer do not share oxygen atoms and a so-called 'spacer' has been introduced (Levin *et al.*, 1998, 2000). In this example, the sequence thus formed consists of slabs of four layers of octahedra along the stacking direction, separated by a spacer. For integer values of *n*, all the slabs have the same width, *n*, but for rational or incommensurate values there are slabs of different numbers of octahedra, *n* being the average number of layers in the slabs. As a result of the vacant M or N layer, the first neighbor of the oxygen atoms closest to the spacer in one slab would be another oxygen atom in the neighboring slab. To avoid electrostatic repulsion between these oxygen atoms, neighboring slabs are found to be shifted 1/2 along the **a** direction with respect to each other. The notation for the atomic layer sequence in this *n* = 4 case can thus be written, MNMN ∅ M′N′M′N′ ∅, where the prime symbol indicates an atomic layer shifted **a**/2 with respect to the original, and the always present O layers have been omitted to simplify the notation, *i.e.* it is assumed that there is always an oxygen layer at the proper position (O or O′) between two M, N, M′, N′ or ∅ layers. Fig. 1(*e*) is a scheme of the layer-stacking sequence for the *n* = 4 case, where the sequence of ideal layers has been explicitly indicated. In general, for the *n* integer, a single period along the **b** direction always contains two slabs of *n* octahedra and two spacers (vacant layers). As the width of a spacer is approximately the width of an octahedron, the length of the unit cell along the stacking direction is thus given by

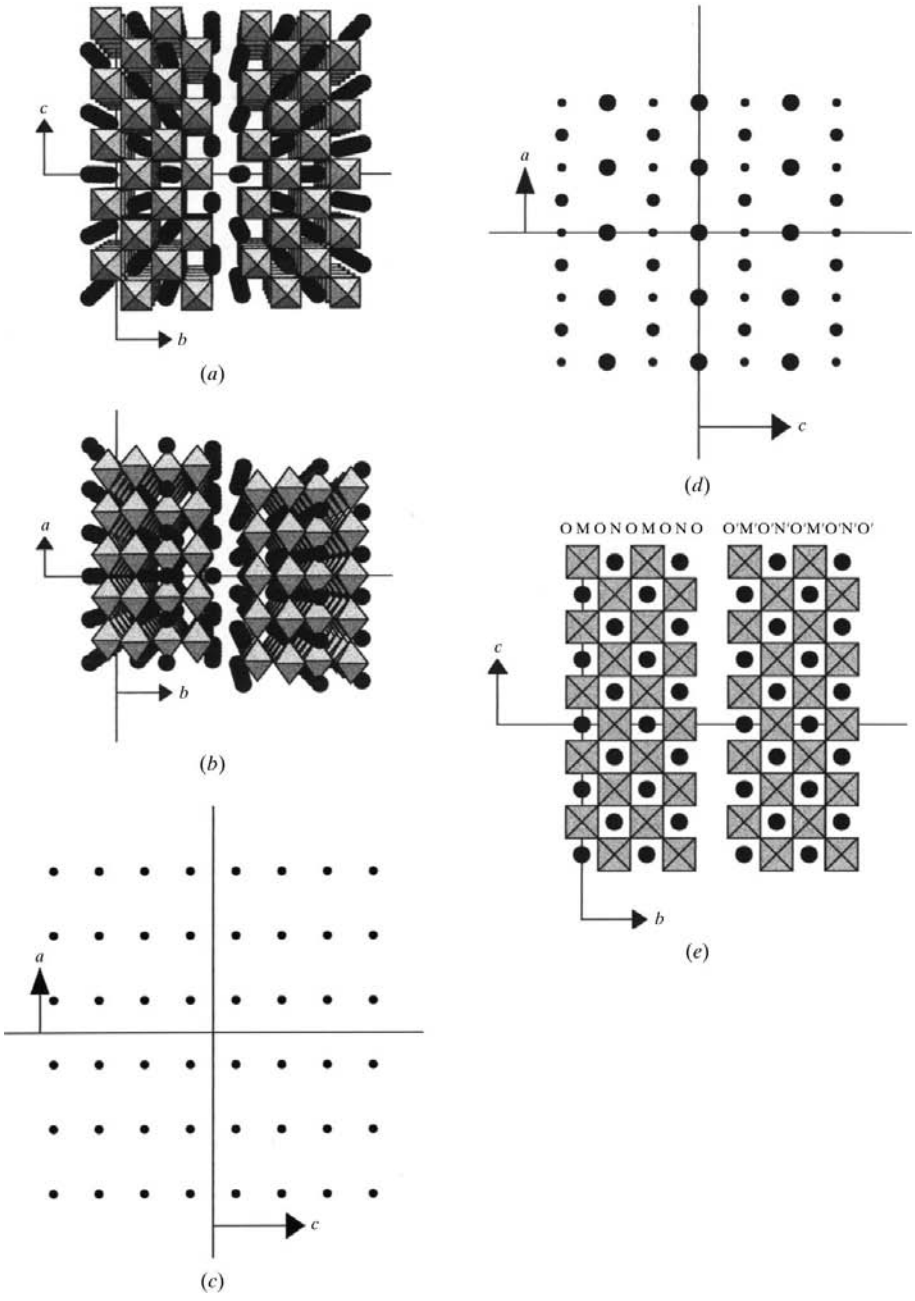

Figure 1
(*a*) and (*b*) Two different views of the structure of the *n* = 4 member of the $Sr_n(Nb, Ti)_nO_{3n+2}$ compound series. $\mathbf{a} = [100]_p$, $\mathbf{b} = [011]_p$ and $\mathbf{c} = [0\bar{1}1]_p$ are the three basis vectors of the average unit cell for the whole compound series (see §3.1). The filled circles represent Sr atoms, while the (Nb,Ti) atoms are located at the centers of the octahedra and the O atoms at the corners of the octahedra. The structure of each member of the compound series $Sr_n(Nb, Ti)_nO_{3n+2}$ consists of the stacking of these layers (in four different relative positions) along the perpendicular **b** axis. The ideal perovskite structure ($n = \infty$) contains a single infinite slab of octahedra. (*c*) Atomic positions within the O layer. The filled circles represent O atoms. The O′ layers are obtained from these O layers *via* an **a**/2 shift. (*d*) Atomic positions within the M layer. The large, intermediate and small filled circles represent Sr, Nb/Ti and O atoms, respectively. M′, N and N′ layers are obtained from this M layer *via* **a**/2, **c**/2 and (**a** + **c**)/2 shifts, respectively. (*e*) Scheme of the ideal layer sequence for the *n* = 4 member of the compound series. The labeling of the atomic layers along the **b** direction has been explicitly indicated.

Table 2
Reported stacking sequences for several members of the $Sr_n(Nb, Ti)_nO_{3n+2}$ compound series.

In the third column, the number of layers of octahedra in each slab of the unit cell is indicated. In the fourth column, the stacking sequence of atomic layers is indicated (see the text).

Composition	n	Sequence of layers of octahedra	Sequence of atomic layers
$Sr_4Nb_4O_{14}$	4	44	MNMN∅M′N′M′N′∅
$Sr_{4.5}Nb_{4.5}O_{15.5}$	4.5	4545	MNMN∅M′N′M′N′M′∅NMNM∅N′M′N′M′N′∅
$Sr_5Nb_5O_{17}$	5	55	MNMNM∅N′M′N′M′N′∅
$Sr_6Nb_6O_{20}$	6	66	MNMNMN∅M′N′M′N′M′N′∅
$Sr_7Nb_7O_{23}$	7	77	MNMNMNM∅N′M′N′M′N′M′N′∅

$b \simeq 2^{1/2}(n+1)a_p$. For rational values of $n = r/s$, the b parameter is then s times greater, $b \simeq 2^{1/2}(r+s)a_p$ and contains $2s$ vacant layers and $2r$ layers of octahedra divided in $2s$ slabs. The reported layer-stacking sequences for some integer and half-integer values are summarized in Table 2. For irrational values of the composition the structure is incommensurate and the b parameter becomes infinite. In the third column of Table 2 the notation of Levin *et al.* (1998) and Levin *et al.* (2000) has been used, where the number of layers of octahedra between succesive spacers is indicated. At $n = 4$, for example, the notation 44 indicates that there are four layers of octahedra following the ideal perovskite packing, a spacer, four layers of octahedra shifted **a**/2 with respect to the previous slab and another spacer within a period. In the fourth column, the previously defined atomic layer notation is used.

This ideal atomic layer-stacking model describes all such structures, but only to a first approximation. Even at the highest temperatures (corresponding to the highest symmetry space groups) the actual atomic positions deviate somewhat from this ideal picture (see for example the deviation of some of the Sr atoms in Figs. 1*a* and *b* from their ideal positions of Fig. 1*e*). The deviations from the ideal positions, however, are constrained by symmetry. Lowering temperature, at any composition, leads to a phase transition whereby some symmetry elements are lost. In Levin *et al.* (1998), Levin & Bendersky (1999) and Levin *et al.* (2000) this high-temperature phase transition is described in terms of tilts of the octahedra around the **a** axis. At still lower temperatures, a further commensurate to incommensurate phase transition occurs for all integer compositions and four-dimensional superspace groups have necessarily been introduced for the description of these incommensurate phases. The number of four-dimensional structure determinations, however, is scarce, due to the difficulty in attaining single crystals for n greater than 5 (Levin *et al.*, 2000) and the low intensity of the observed satellite reflections. To the best of our knowledge, a superspace-group structure determination has only been performed for the compounds $Sr_2Nb_2O_7$ ($n = 4$; Yamamoto, 1982; Levin *et al.*, 2000) and $(Nd_4Ca_2)Ti_6O_{20}$ (Nanot *et al.*, 1986; Grebille & Berar, 1987). (The latter phase is isomorphous to the $n = 6$ member of the compound series.) In both cases the reported superspace group was $Cmc2_1(\gamma'00)0s0$. The $n = 5$ member of the series ($Sr_5Nb_4TiO_{17}$) has been analyzed by means of electron diffraction and the assigned superspace group was $Pmnn(\gamma'00)000$. In addition, the average structures of the $n = 4$ (Ishizawa *et al.*, 1975) and $n = 5$ (Drews *et al.*, 1996; Abrahams *et al.*, 1998) members of the compound series have also been determined.

3. The superspace description

The fact that the layer-stacking sequences depend on composition and follow a well defined rule so that the spacers are as homogeneously distributed as possible (homogeneous sequence; Levin *et al.*, 2000) is a clear indication that the structure can be uniquely described by a single superspace model. The suitability of a superspace description is also suggested by the presence in experimental electron diffraction patterns of a common subset of strong parent reflections, accompanied by a subset of composition-dependent 'satellite' reflections, as occurs in similar systems (Perez-Mato *et al.*, 1999; Elcoro *et al.*, 2000).

As stressed in the previous section, a complete conventional description of the set of phase transitions for a compound of Table 1 must include the space group of the 'untilted' phase at high temperature, the space group of the tilted phase at lower temperature, the four-dimensional superspace group of the incommensurate structure and the space group of the lock-in phase at low temperature. Although the relationship between the symmetries for different compositions can be analyzed in the standard crystallographic approach (Levin & Bendersky, 1999), the superspace formalism offers a more unified description for the whole family. Here we will show that it is possible to describe the high-temperature untilted structure for all compositions by means of a unique four-dimensional superspace group with a composition-dependent modulation vector parallel to the layer-stacking direction (for a short practical introduction to the use of the superspace approach see Perez-Mato *et al.*, 1987). The phase transition to the tilted structures is then described by a reduction of the symmetry into another four-dimensional superspace group, a subgroup of the initial (high-temperature) one. This second superspace symmetry is also composition independent. At lower temperatures, the introduction of an additional displacive modulation parallel to the **a** axis necessitates the use of a five-dimensional superspace group. Finally, the lock-in phase transition at low temperature returns the description to four dimensions. Therefore, at any temperature, a unique model for the whole family requires an extra dimension with respect to the standard approach.

3.1. High-temperature phases (untilted phases)

As a first step we determine the set of occupational atomic domains in superspace which give rise to the observed layer-

Table 3
General structural parameters in the superspace description of the high-temperature common structure with superspace group $F'mmm(0\gamma0)000$.

Superscript a represents antisymmetric functions.

Element	x_1	x_2	x_3	x_4	Width of the atomic domain	Point symmetry	Displacive modulation
Sr	0	0	0	0	$(1-\gamma)/2$	*mmm*	$[0, x_2^a(x_4), 0]$
Nb/Ti	$\frac{1}{2}$	0	$\frac{1}{2}$	0	$(1-\gamma)/2$	*mmm*	$[0, x_2^a(x_4), 0]$
O1	0	0	$\frac{1}{2}$	0	$(1-\gamma)/2$	*mmm*	$[0, x_2^a(x_4), 0]$
O2	$\frac{1}{2}$	$\frac{1}{4}$	$\frac{1}{4}$	0	$\frac{1}{2}$	$2/m11$	$[0, x_2^a(x_4), x_3^a(x_4)]$

Table 4
Symmetry operations of the superspace group $F'mmm(0\gamma0)000$ and resulting reflection conditions.

$\{E, 1\|000, 0\}$	x_1, x_2, x_3, x_4	$\{I, \bar{1}\|000, 2\varphi\}$	$\bar{x}_1, \bar{x}_2, \bar{x}_3, 2\varphi - x_4$
$\{m_x, 1\|000, 0\}$	$\bar{x}_1, x_2, x_3, x_4$	$\{2_x, \bar{1}\|000, 2\varphi\}$	$x_1, \bar{x}_2, \bar{x}_3, 2\varphi - x_4$
$\{2_y, 1\|000, 0\}$	$\bar{x}_1, x_2, \bar{x}_3, x_4$	$\{m_y, \bar{1}\|000, 2\varphi\}$	$x_1, \bar{x}_2, x_3, 2\varphi - x_4$
$\{m_z, 1\|000, 0\}$	$x_1, x_2, \bar{x}_3, x_4$	$\{2_z, \bar{1}\|000, 2\varphi\}$	$\bar{x}_1, \bar{x}_2, x_3, 2\varphi - x_4$
$\{E, 1\|\frac{1}{2}\frac{1}{2}0, \frac{1}{2}\}$	$\frac{1}{2}+x_1, \frac{1}{2}+x_2, x_3, \frac{1}{2}+x_4$		
$\{E, 1\|\frac{1}{2}0\frac{1}{2}, \frac{1}{2}\}$	$\frac{1}{2}+x_1, x_2, \frac{1}{2}+x_3, \frac{1}{2}+x_4$		
$\{E, 1\|0\frac{1}{2}\frac{1}{2}, 0\}$	$x_1, \frac{1}{2}+x_2, \frac{1}{2}+x_3, x_4$		

Reflection conditions
$(h\ k\ l\ m)$ $\quad k+l=$ even
$(h\ k\ l\ m)$ $\quad h+k+m=$ even

Table 5
Space groups for commensurate structures with rational $\gamma = r/s$ and superspace group $F'mmm(0\gamma0)000$ [$\gamma = 1/(n+1)$].

r = odd s = odd (n = 4, 6)	$\varphi = 0$ (mod. $1/2s$) *Cmmm*	$\varphi = \frac{1}{4}$ (mod. $1/2s$) *Cmcm*	$\varphi =$ arbitrary *Cm2m*
r = odd s = even (n = 5)	$\varphi = 0$ (mod. $1/2s$) *Immm*	$\varphi = 1/4s$ (mod. $1/2s$) *Imcm*	$\varphi =$ arbitrary *Im2m*
r = even s = odd (n = 4.5)	$\varphi = 0$ (mod. $1/2s$) *Ammm*	$\varphi = \frac{1}{4}$ (mod. $1/2s$) *Amam*	$\varphi =$ arbitrary *Am2m*

stacking sequences at high temperatures and the corresponding composition-dependent primary modulation wavevector. Then, a unique four-dimensional superspace group will be assigned to this construction. This superspace construction must be capable of explaining all conventional space groups observed for whatever composition. For this purpose, it is convenient to take as a reference structure the $n = \infty$ ideal perovskite structure. As described in the previous section, viewed along the $[011]_p$ direction, the layer-stacking sequence of the ideal perovskite structure is MNMN... . It can be easily verified, once the notation is understood, that the superspace model shown in Fig. 2 correctly represents the layer-stacking sequence of the ideal perovskite structure. The figure is a two-dimensional projection of a superspace unit cell on the $x_2 - x_4$ (or $y - x_4$) plane. The average lattice is defined by the two vectors which span an atomic layer, $a \simeq a_p = 3.933$ Å, $c \simeq 2^{1/2}a_p = 5.562$ Å and the width of two octahedra along y, $b \simeq 2^{1/2}a_p = 5.562$ Å. The horizontal axis in the figure is the stacking direction, parallel to the **b** axis, while the vertical axis is the internal subspace. Dark red, light red, dark blue and light blue AS's represent the M, N, M′ and N′ layers, respectively, *i.e.* they represent all the atoms included in each layer at the corresponding (x, z) positions. Dark and light green AS's represent O and O′ layers, respectively. A horizontal section perpendicular to x_4 and containing the origin thus gives the correct layer stacking sequence MNMNMN... . Shifting the origin along the internal subspace does not introduce any change in the real structure, apart from a global shift $(\mathbf{a} + \mathbf{c})/2$ of the whole structure, whenever the limits of the AS's are crossed. The width along the internal subspace of all the AS's for this $n = \infty$ ideal perovskite composition is $\frac{1}{2}$ and the magnitude of the modulation wavevector is zero.

For any other composition, $Sr_n(Nb, Ti)_nO_{3n+2}$, there must be one vacant Sr(Ti,Nb)O layer for each $n + 1$ layers. In principle, this argument can be extended to non-integer compositions, *i.e.* the stoichiometric formula can be rewritten as $[Sr(Ti, Nb)O]_{(1-\gamma)}O_2$, where $\gamma = 1/(n+1)$ is real. In the general case, there should be a concentration of γ vacant Sr(Ti,Nb)O layers and M′ and N′ layers will necessarily enter into the layer stacking sequence. Both requirements are achieved in superspace by reducing the width of the AS's to reproduce the required composition while simultaneously changing the magnitude of the modulation wavevector. For the general composition $[Sr(Ti, Nb)O]_{(1-\gamma)}O_2$, the width representing the M, N, M′ and N′ layers is reduced to $(1-\gamma)/2$, while the AS's representing the O_2 layers (the green vertical bars in Fig. 2) remain unchanged. Fig. 3 is an example of the appropriate superspace construction for the $n = 5$ ($\gamma = 1/6$) member of the series, where the same projection as the one used in Fig. 2 is shown. The introduction of a modulation vector different from zero shifts neighboring sets of Sr(Nb,Ti)O atomic surfaces relative to one another along internal space and leads to a breakdown in perfect perovskite-like ordering when a horizontal section perpendicular to x_4 is taken. As has been previously stressed, vacancy layers are accomodated between neighboring slabs of perfect perovskite. Fig. 3 can also be used to deduce the appropriate value of the modulation vector for any particular composition. It is straightforward to demonstrate that the composition-dependent modulation wavevector must be $\mathbf{q} \equiv \gamma\mathbf{b}^*$ ($\gamma = 1/6$ in the particular case of Fig. 3). A lower value would give rise to two consecutive layers of vacancies, not experimentally observed and crystal chemically unreasonable (three consecutive O_2 layers would be present in the sequence). A greater value would produce pairs, MM′ and NN′, configurations which represent another type of local coordination polyhedron, never experimentally observed. It can easily be checked that the superspace construction sketched in Figs. 2 and 3 with the composition-dependent magnitude of the modulation wavevector reproduces the stacking sequences experimentally observed and shown in Table 2.

The average structure at any composition thus has *Fmmm* symmetry, four Sr and four (Nb,Ti) atoms with occupation probability $(1-\gamma)/2$, four O atoms with occupation probability $(1-\gamma)/2$ and another eight O atoms with occupation probability 1. Their positions within the superspace unit cell

are given in Table 3 along with the other structural parameters of the superspace construction, valid for any member of the compound series at high temperatures.

Once the relationship between composition and modulation wavevector is known, it is interesting to investigate possible limiting values for the modulation wavevector magnitude, γ. For the $Sr_n(Nb, Ti)_nO_{3n+2}$ compound series, the range of γ is fixed by the limits on the composition range. As $4 \leq n \leq \infty$, the modulation wavevector magnitude, γ, will be constrained to the range $0 \leq \gamma \leq 1/5$. However, $n = 2$ ($\gamma = 1/3$) members are known for the isomorphous compounds, $BaMF_4$ (M = Mg, Mn, Fe, Co, Zn, Cu; see Table 1 in Levin & Bendersky, 1999). For $1/2 < \gamma$ values three consecutive O layers would be present, which is clearly unreasonable from the electrostatic point of view. Finally compositions in the range $\frac{1}{3} < \gamma < \frac{1}{2}$ would give rise to isolated layers of octahedra, surrounded by two vacant layers. This configuration accumulates an excess of negative charge (a single M/N layer sandwiched between two pairs of O layers) and probably, for this composition range, the system would prefer another configuration.

3.1.1. Superspace group of the high-temperature phase. The superspace construction outlined above is valid for any particular composition. A most important point is that the associated superspace-group symmetry proves to be unique and composition independent, as occurs in similar systems (Perez-Mato *et al.*, 1999; Elcoro *et al.*, 2000). This unique superspace group of the highest temperature phases can be denoted as $F'mmm(0, \gamma, 0)000$, $Fmmm(1, \gamma, 0)000$ in the conventional setting (Janssen *et al.*, 1992), where the symbol F' represents the three non-standard centering operations in superspace: $(\frac{1}{2},\frac{1}{2},0,\frac{1}{2})$, $(\frac{1}{2},0,\frac{1}{2},\frac{1}{2})$ and $(0,\frac{1}{2},\frac{1}{2},0)$. This high-symmetry superspace group has 32 symmetry operations, given in (x_1, x_2, x_3, x_4) coordinates in Table 4, and corresponding to the periodic basis of superspace. The relationship between these coordinates and the real space-internal space coordinates are $x = x_1$, $y = x_2$, $z = x_3$, $t = x_4 - \gamma x_2$. Table 4 defines unambiguously this superspace group by listing its symmetry operations and the resulting reflection conditions. Note that some of the four-dimensional symmetry operations in Table 4 contain a global phase φ, which for an incommensurate phase can be arbitrarily chosen. However, for a commensurate modulation (*i.e.* rational γ) the value of this global phase is important for the resulting conventional three-dimensional space-group symmetry. The possible three-dimensional space groups for a given rational modulation wavevector magnitude and global phase φ can be derived from the common superspace group for the whole series by applying simple algebraic rules (Perez-Mato, 1992). A continuous shift of section (a continuous change of the global phase φ) does not change the resulting space group unless the phase takes some γ-dependent set of special rational values. For those cases the resultant three-dimensional space group has a higher symmetry. However, due to the discontinuity of the crenel functions used to represent the AS's, the section corresponding to a specific value of the global phase φ should not contain a boundary of an AS, *i.e.* only physical sections through points where all the AS's are continuous are relevant in this model. Otherwise, problems with the symmetry and/or stoichiometry arise. This situation is different from what happens in standard incommensurately/commensurately modulated structures, where the AS's are usually continuous and all sections, all values of φ, are possible. The different possible resultant three-dimensional space groups as a function of the various possible rational modulation wavevectors (rational compositions) are listed in Table 5. The experimentally reported space groups for the high-temperature phases are *Cmcm*, *Immm* and *Ammm* for

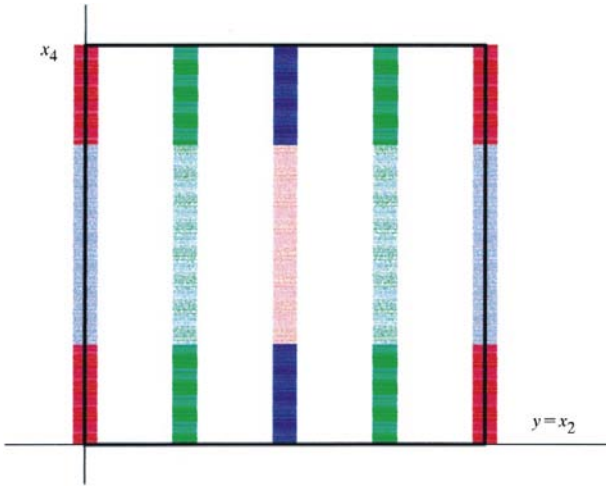

Figure 2
The set of atomic surfaces in the superspace construction for the ideal perovskite structure $[(y, x_4) \equiv (x_2, x_4)$ projection]. Dark red, light red, dark blue, light blue, dark green and light green represent M, M′, N, N′, O and O′ atomic layers, respectively. The modulation parameter for this ideal perovskite case is $\gamma = 0$.

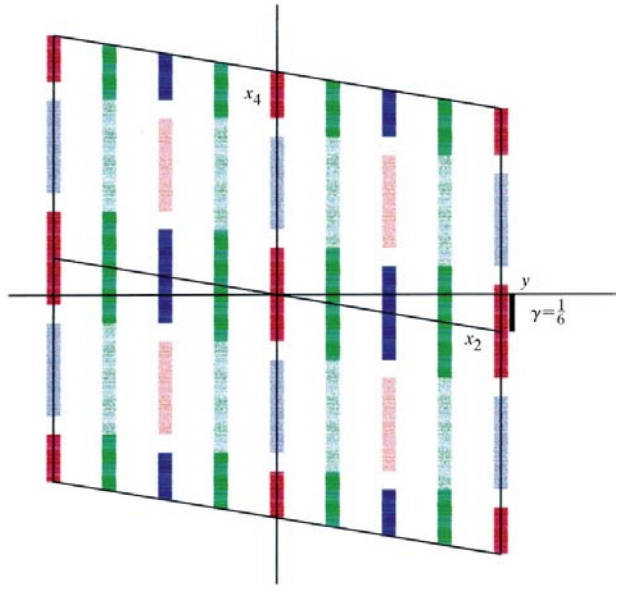

Figure 3
The set of atomic surfaces in superspace for the $n = 5$ member of the compound series $[(y, x_4) \equiv (x_2, x_4)$ projection]. The key for the colors is the same as in Fig. 2. The modulation wavevector magnitude for this $n = 5$ case is $\gamma = 1/6$. Four superspace unit cells have been included to make more clear the resulting layer stacking sequence.

Table 6
Symmetry operations of the superspace group $C'mcb(0\gamma0)000(\gamma'00)0s0$ and resulting reflection conditions.

$\{E, 1, 1\|000, 0, 0\}$	x_1, x_2, x_3, x_4, x_5
$\{m_x, 1, \bar{1}\|000, 0, \frac{1}{2}+2\varphi'\}$	$\bar{x}_1, x_2, x_3, x_4, \frac{1}{2}+2\varphi'-x_5$
$\{2_y, 1, \bar{1}\|0\frac{1}{2}\frac{1}{2}, 0, \frac{1}{2}+2\varphi'\}$	$\bar{x}_1, \frac{1}{2}+x_2, \frac{1}{2}-x_3, x_4, \frac{1}{2}+2\varphi'-x_5$
$\{m_z, 1, 1\|0\frac{1}{2}\frac{1}{2}, 0, 0\}$	$x_1, \frac{1}{2}+x_2, \frac{1}{2}-x_3, x_4, x_5$
$\{E, 1, 1\|\frac{1}{2}\frac{1}{2}0, \frac{1}{2}, 0\}$	$\frac{1}{2}+x_1, \frac{1}{2}+x_2, x_3, \frac{1}{2}+x_4, x_5$
$\{I, \bar{1}, \bar{1}\|000, 2\varphi, 2\varphi'\}$	$\bar{x}_1, \bar{x}_2, \bar{x}_3, 2\varphi-x_4, 2\varphi'-x_5$
$\{2_x, \bar{1}, 1\|000, 2\varphi, \frac{1}{2}\}$	$x_1, \bar{x}_2, \bar{x}_3, 2\varphi-x_4, \frac{1}{2}+x_5$
$\{m_y, \bar{1}, 1\|0\frac{1}{2}\frac{1}{2}, 2\varphi, \frac{1}{2}\}$	$x_1, \frac{1}{2}-x_2, \frac{1}{2}+x_3, 2\varphi-x_4, \frac{1}{2}+x_5$
$\{2_z, \bar{1}, \bar{1}\|0\frac{1}{2}\frac{1}{2}, 2\varphi, 2\varphi'\}$	$\bar{x}_1, \frac{1}{2}-x_2, \frac{1}{2}+x_3, 2\varphi-x_4, 2\varphi'-x_5$
Reflection conditions	
$(h\ k\ l\ m\ m')$	$h+k+m=$ even
$(h\ k\ 0\ m\ m')$	$k=$ even
$(h\ 0\ l\ 0\ m')$	$l+m'=$ even

n = even, odd and half-integer, respectively (Levin & Bendersky, 1999; Levin *et al.*, 2000). For n = odd (γ = odd/even) and n = half-integer (γ = even/odd), these space groups correspond to $\varphi = 0$ in Table 5. For n = even (γ = odd/odd), however, the $\varphi = 0$ section contains limits of some of the AS's. As stressed above, it is therefore avoided by the system. The relevant real-space section taken corresponds to $\varphi = 1/4$ and its equivalents, giving rise to resultant *Cmcm* space-group symmetry, in agreement with Levin & Bendersky (1999). In this latter case, the inversion center is located in a vacant layer.

The AS's are not forced to be vertical lines. In other words, the atoms can shift from their ideal positions in a layer, provided they maintain the superspace symmetry of the structure. To extend the analysis beyond the ideal picture of Figs. 2 and 3, we must include the set of displacive atomic modulation functions which describe the static displacements of the atoms in each cell from their idealized average layer-like values. The symmetry of these displacive modulations is determined by the point-group symmetry at the center of the relevant atomic domain. Very simple algebraic rules lead to the most general form of these AS's (see, for example, Section 5 in Elcoro *et al.*, 2000). The seventh and eighth columns in Table 3 show the point symmetry of the various AS's and the general functions which describe them. The first three AS's in the table have *mmm* point symmetry which restricts their form to be an antisymmetric function contained in the $y - x_4$ plane. The form of the fourth AS corresponding to the oxygen layers (the green bars in Fig. 2) is less restricted and has two components: the same antisymmetric modulation as the other AS's and an antisymmetric modulation parallel to the z axis.

3.2. Phases at lower temperature (tilted phases and incommensurate phases)

As indicated in Table 1, for all compositions there is an initial phase transition from the highest-temperature untilted orthorhombic phase to a state of lower symmetry upon lowering the temperature. This phase transition is due to a tilting of the octahedra around the **a** axis (Levin & Bendersky, 1999; Levin *et al.*, 2000), causing some atoms in the high-temperature unit cell to move from their ideal positions, in a different way from that allowed in the eighth column of Table 3, so that a genuine symmetry breaking occurs. In all the cases known the m_z symmetry element is lost. For n = odd and n = half-integer the centering of the unit cell is also lost (see Table 1). In the superspace description there is also a lowering of symmetry, but it does not imply any change of the unit-cell parameters or the width of the AS's, so that the unit cell of the overall average structure is defined by the same set of three basis vectors as the high-temperature phase. However, the loss of some symmetry elements increases the number of independent atoms in the unit cell. The resulting four-dimensional superspace group is a subgroup of the four-dimensional superspace group at high temperatures, as given in Table 4. Upon further lowering of temperature, a second phase transition occurs at which an extra incommensurate modulation parallel to the $\mathbf{a}^*$ axis appears, which requires the superspace analysis to move up to five dimensions. As the structure of the tilted phase is the average structure of the incommensurate phase, we focus our analysis on the description of the incommensurate structure. The determination of the superspace group of this phase must be achieved using the experimental information available, *i.e.* the published electron diffraction patterns and the reported four-dimensional superspace groups given in Table 1. The five-dimensional superspace group we are looking for must give rise to the experimentally reported four-dimensional superspace groups for the known rational members of the compound series (shown in Table 1). The knowledge of these symmetries is therefore a very important clue as to the relevant five-dimensional superspace group. The diffraction patterns obtained from the literature have thus been re-indexed using the relevant five reciprocal space basis vectors. The corresponding systematic extinctions indicate what is the superspace group. In our analysis we have used the published electron diffraction patterns for the n = 4, 5, 6, 7 members of the $Sr_n(Nb, Ti)_nO_{3n+2}$ compound series of Levin *et al.* (2000). A careful analysis of these diffraction patterns indicates that the relevant five-dimensional superspace group for the whole compound series is $C'mcb(0\gamma0)000(\gamma'00)0s0$. The C' symbol represents the non-standard centering operation ($\frac{1}{2}$, $\frac{1}{2}$, 0, $\frac{1}{2}$, 0). The two modulation vectors are $\mathbf{q} = \gamma\mathbf{b}^*$ and $\mathbf{q}' = \gamma'\,\mathbf{a}^*$, and each reflection in the diffraction pattern can be indexed by means of five indices

$$\mathbf{H} = h\mathbf{a}^* + k\mathbf{b}^* + l\mathbf{c}^* + m\mathbf{q} + m'\mathbf{q}'. \qquad (1)$$

The first modulation wavevector is composition-dependent and its modulus has the same value as in the high-temperature phase. The second modulation wavevector appears when

lowering the temperature and its modulus has an irrational value close to 0.5 for all compositions (Levin *et al.*, 2000). The subset of satellite reflections $m' = 0$ constitutes the diffraction pattern of the average structure of the incommensurate phase and provides information as to the structure of the tilted phases. Table 6 lists the elements of this five-dimensional superspace group $C'mcb(0\gamma0)000(\gamma'00)0s0$ along with the corresponding reflection conditions. Removing the fifth component of both rotational and translational parts of the elements of this table leads to the symmetry elements of the four-dimensional superspace group $C'mcb(0\gamma0)000$ of the tilted phase.

At this stage it is interesting to compare the experimentally reported space (superspace) groups for the tilted (incommensurate) phases with the resulting symmetries compatible with the superspace group of Table 6. The possible four-dimensional superspace groups of the incommensurate phases for any rational composition (rational modulation wavevector γ), given the composition-independent five-dimensional superspace group $C'mcb(0\gamma0)000(\gamma'00)0s0$, are summarized in Table 7. The space groups of the tilted phases for all rational compositions are the corresponding space groups of the average structures. They can be deduced from Table 7 by removing the modulation vector and internal translations associated with the symmetry elements.

For n = even (γ = odd/odd) the reported superspace group is $Cmc2_1(\gamma'00)0s0$ (see Table 1), which corresponds to $\varphi = \frac{1}{4}$ in Table 7 and coincides with the value taken at high temperatures. The experimental space group of the tilted phases is thus $Cmc2_1$. By contrast, for n = odd (γ = odd/even), while the experimental space group of the tilted phases coincides with the resulting space group for $\varphi = 0$ in Table 7, *Pmnn*, the reported superspace group for the incommensurate phase, $Pmnn(\gamma'00)000$ (Levin *et al.*, 2000), does not match any resulting superspace group in Table 7. Table 7, for φ = 0, gives a superspace group $Pmnn(\gamma'00)0s0$, which differs from the reported one only in the translation along internal space associated with the mirror plane perpendicular to the y axis. A careful analysis of the diffraction pattern for n = 5 in Fig. 2(*a*) of Levin *et al.* (2000), however, shows that the two reflections marked with an arrow are the satellites (001 $\pm$1) which, in principle, are systematic extinctions in the superspace group reported by Levin *et al.* (2000), but they are not in the superspace group of Table 7 (see also Fig. 4*b*). The assigned superspace group of Levin *et al.* (2000) must therefore be corrected. We conclude that the correct five-dimensional superspace group must be

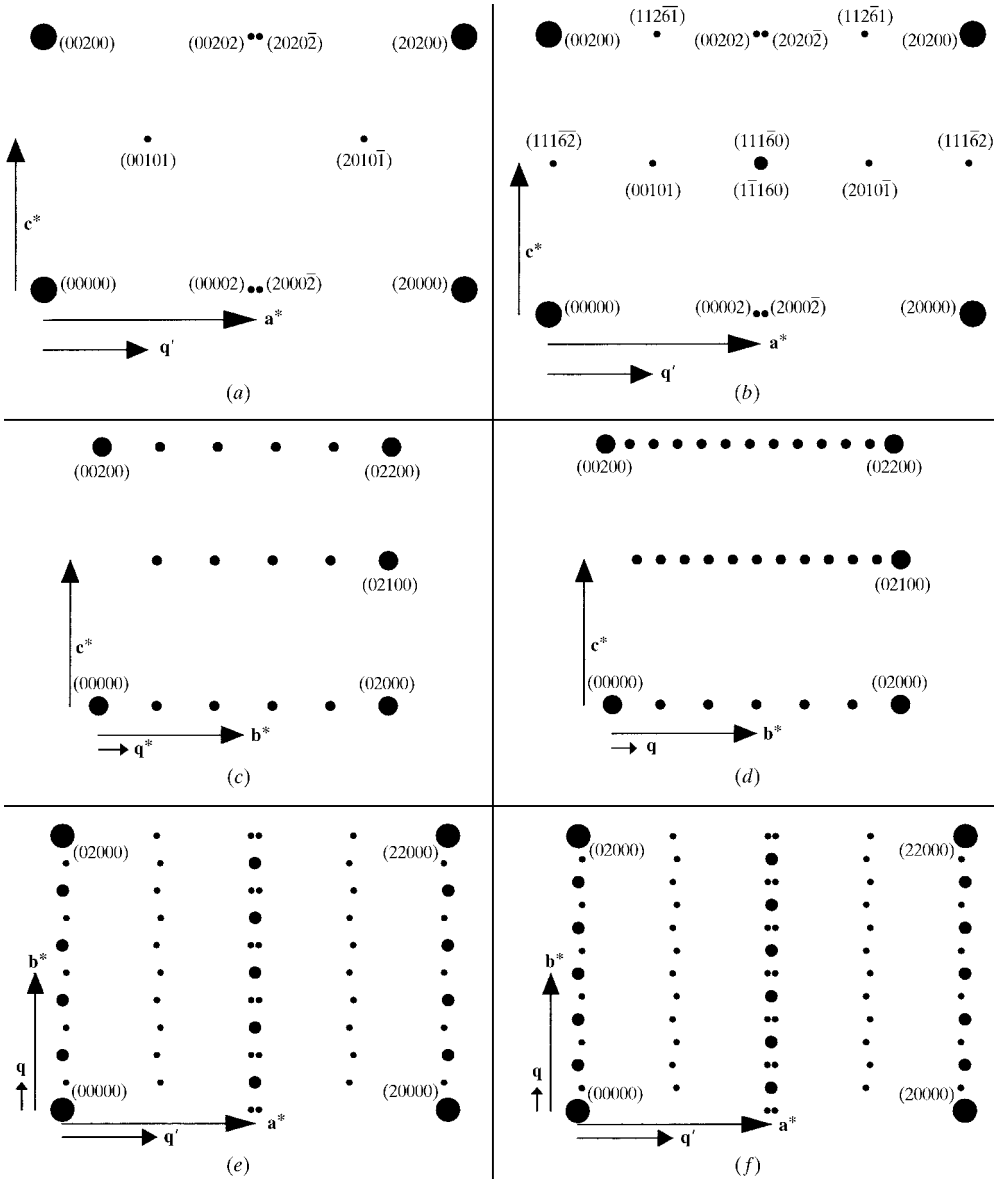

Figure 4
Schematic diagrams of the three major sections of reciprocal space of the $\mathbf{b} = [011]_p$ and $\mathbf{c} = [0\bar{1}1]_p$ family of compounds compatible with the superspace group $C'mcb(0, \gamma, 0)000(\gamma', 0, 0)0s0$. (*a*), (*c*) and (*e*) represent the three sections ($\mathbf{a}^*$, $\mathbf{c}^*$), ($\mathbf{b}^*$, $\mathbf{c}^*$) and ($\mathbf{a}^*$, $\mathbf{b}^*$) for the composition $n = 4$ and $\varphi = 0$. (*b*), (*d*) and (*f*) represent the same sections for $n = 5$ and $\varphi = \frac{1}{4}$. The large filled circles represent the reflections which are in common for all compositions [corresponding to the overall average structure, *i.e.* with $m = m' = 0$ in (1)], the intermediate filled circles represent the $m' = 0$ reflections, while the small filled circles represent the incommensurate satellite reflections up to $|m'| \leq 2$.

$C'mcb(0\gamma0)000(\gamma'00)0s0$ as it fits all experimental symmetry results.

Fig. 4 reproduces in a schematic way the three major sections of reciprocal space compatible with the superspace group $C'mcb(0\gamma0)000(\gamma'00)0s0$ for the $n = 4$ and $n = 5$ cases. In these diagrams the reflections have been divided into three categories. Large circles represent main reflections, corresponding to the global average structure for all compositions [$m = m' = 0$ in (1)]. Intermediate circles represent satellite reflections due to the composition-dependent modulation wavevector, *i.e.* reflections with $m' = 0$ in (1). As previously stressed, this subset of reflections, together with the principal reflections, represents the reciprocal lattice characteristic of both the tilted structure and the average structure of the incommensurately modulated phase (superspace group $C'mcb(0\gamma0)000$). Finally, the smallest circles represent satellite reflections of the incommensurately modulated structure, $m' \neq 0$, up to second order, $|m'| \leq 2$. The similarities between these schematic diffraction patterns and the experimental electron diffraction patterns of Levin *et al.* (2000) are evident, but the interpretation of the diagrams requires some additional comment. The sections parallel to ($\mathbf{a}^*$, $\mathbf{b}^*$) and ($\mathbf{b}^*$, $\mathbf{c}^*$) for $n = 4$ (Figs. 4*c* and 4*e*) and $n = 5$ (Figs. 4*d* and *f*) are rather similar. As the modulation vector is $\mathbf{q} = \mathbf{b}^*/5$ in the first case and $\mathbf{q} = \mathbf{b}^*/6$ in the latter case, the line joining the (00000) and the (02000) main reflections is divided into 10 and 12 parts, respectively. Not all potential reflections are present, however, because of systematic extinction conditions. The sections parallel to ($\mathbf{a}^*$, $\mathbf{c}^*$), however (Fig. 4*a* for $n = 4$ and Fig. 4*b* for $n = 5$), are not so similar. At the center of Fig. 4(*b*) there is an intense spot at the position of the main reflection (10100), but according to Table 6 this reflection should be forbidden because of the centering operation. However, due to the commensurability of the composition-dependent modulation, some other reflections which are not systematically extinct

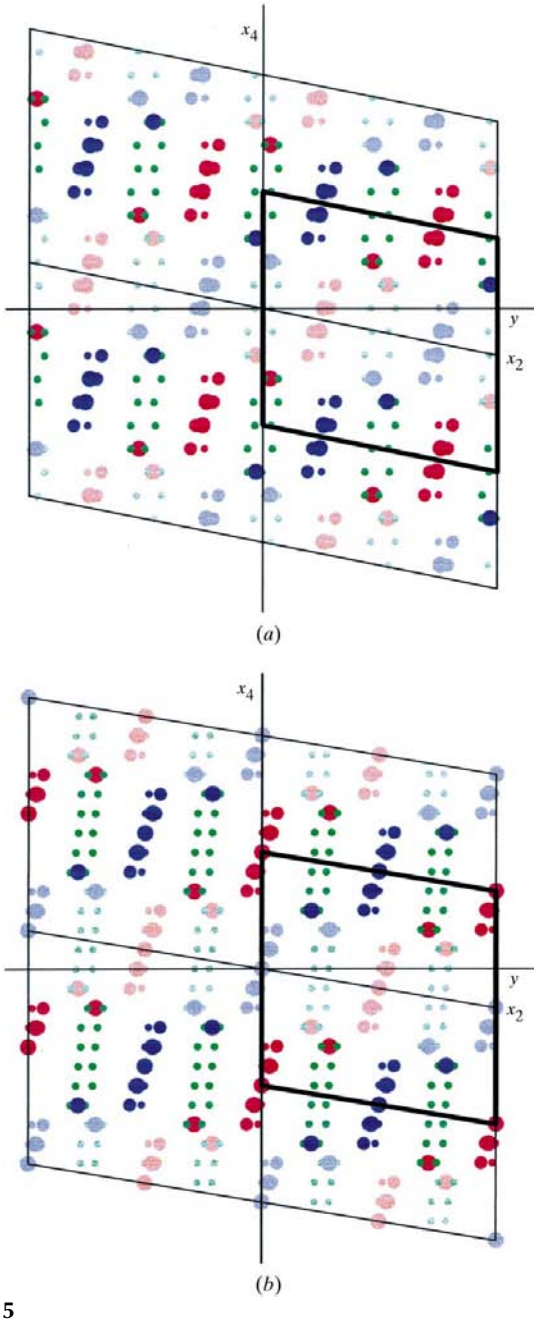

Figure 5
$x_2 - x_4$ ($y - x_4$) projection of the superspace reconstruction for the tilted phase of the (*a*) $Sr_2Nb_2O_7$ ($n = 4$) and (*b*) $Sr_5Nb_5O_{17}$ ($n = 5$) compounds from Ishizawa *et al.* (1975) and Abrahams *et al.* (1998), respectively. The large, intermediate and small filled circles represent Sr, Nb and O atoms, respectively, and the key for the colors is the same as in Figs. 2 and 3. Four superspace unit cells have again been included to make clear the interlayer stacking sequences. The unit cell corresponding to the choice of origin in Figs. 2 and 3 has been outlined. In (*a*) the relevant section is $\varphi = 9/20$, equivalent to $\varphi = \frac{1}{4}$ for $\gamma = r/s$ = odd/odd (see Table 7 and the text). In (*b*) the relevant section is $\varphi = \frac{1}{2}$, equivalent to $\varphi = 0$ for $\gamma = r/s$ = odd/even.

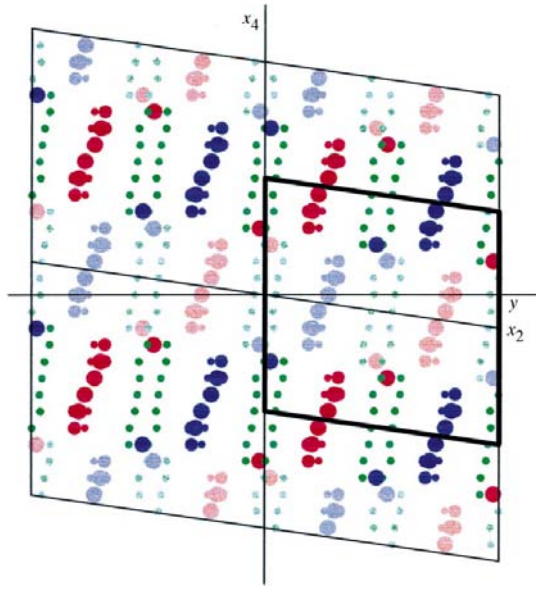

Figure 6
The same superspace projection as in Fig. 5 for $Nd_4Ca_2Ti_6O_{20}$ (a compound isomorphous to an $n = 6$ compound) derived from the atomic positions of Grebille & Berar (1987). The large, intermediate and small filled circles represent (Nd,Ca), Ti and O atoms, respectively. The relevant section is $\varphi = 11/28$, equivalent to $\varphi = \frac{1}{4}$ for $\gamma = r/s$ = odd/odd (see Table 7 and the text).

Table 7
Four-dimensional superspace groups for incommensurate structures with rational $\gamma = r/s$ and five-dimensional superspace group $C'mcb(0\gamma0)000(\gamma'00)0s0$ [$\gamma = 1/(n+1)$].

r = odd s = odd (n = 4, 6)	$\varphi = 0$ (mod. $1/2s$) $C2/m11(\gamma'00)0$	$\varphi = \frac{1}{4}$ (mod. $1/2s$) $Cmc2_1(\gamma'00)0s0$	φ = arbitrary $Cm11(\gamma'00)0$
r = odd s = even (n = 5)	$\varphi = 0$ (mod. $1/2s$) $Pmnn(\gamma'00)0s0$	$\varphi = 1/4s$ (mod. $1/2s$) $Pmcn(\gamma'00)0s0$	φ = arbitrary $Pm2_1n(\gamma'00)000$
r = even s = odd (n = 4.5)	$\varphi = 0$ (mod. $1/2s$) $Pmcb(\gamma'00)0s0$	$\varphi = \frac{1}{4}$ (mod. $1/2s$) $Pmnb(\gamma'00)0s0$	φ = arbitrary $Pm2_1b(\gamma'00)000$

[satellite reflections with $m \neq 0$ and $m' = 0$ in (1)] occur at the same position of the diffraction pattern. The allowed satellite reflections of the lowest harmonic order at that position are $(11\bar{6}0)$ and $(1\bar{1}160)$. By contrast, for the case $n = 4$, the satellites of lowest order which fall at that position are $(11\bar{5}0)$ and $(1\bar{1}150)$, respectively. Both reflections are forbidden by the five-dimensional superspace group (see Table 6). The intensity at that point is therefore zero. The same happens with other reflections in these diagrams: some satellite reflections which are not systematically extinct are present in the ($\mathbf{a}^*$, $\mathbf{c}^*$) section for n = even, but forbidden for n = odd, while for some other reflections the opposite occurs. Determining the resultant space group from a superspace group depends not only on observed systematic extinctions, but also on the value of the phase φ in Table 7, *i.e.* the space group of the real structure depends on the height of the horizontal cut made in the superspace construction to obtain the atomic positions. According to the experimental evidence of the space groups reported for the $n = 4$ and $n = 5$ compositions ($Cmc2_1$ and $Pmnn$, respectively), the chosen value of the global phase is given by $\varphi = \frac{1}{4}$ and $\varphi = 0$, respectively (see Table 7). As a consequence of these values, in some cases symmetry-related satellite reflections which fall at the same point as a forbidden main reflection have a phase difference of π and the superposition has zero intensity, maintaining the systematic extinction. For example, in Fig. 4(*a*) the two reflections $(01\bar{5}0)$ and $(0\bar{1}150)$, which are not individually forbidden, fall at the same point of reciprocal space as the systematically extinct (00100). Both reflections are related by the symmetry element $\{m_y, \bar{1}, 1|0, 1/2, 1/2, 2\phi, 1/2\}$ in Table 6 and, as the relevant value for n = even is $\varphi = \frac{1}{4}$, the phase difference of the scattering factors associated with these reflections is π and the systematic extinction is maintained. Note that a different value for the phase φ ($\varphi = 0$ or equivalent or φ = arbitrary) would not maintain this extinction and the resulting space group would be different (see Table 7).

In the standard crystallographic description all the $m' = 0$ reflections in (1) are considered main reflections and the three basis vectors of the reciprocal lattice of the average structure are taken to be $\mathbf{a}^{*'} = \mathbf{a}^*, \mathbf{b}^{*'} = \gamma\mathbf{b}^*, \mathbf{c}^{*'} = \mathbf{c}^*$. As a consequence, the systematic extinction conditions are different for n = even and n = odd. The corresponding space groups of the average structures are therefore also different.

The final structural parameters corresponding to this superspace model are summarized in Table 8. Note that one of the independent atoms (the O atom represented by the green AS's in Fig. 2 or 3) does not occupy such a special position as it did in the high-temperature phase (Table 3). The center of the AS has two refinable parameters. The point groups of the AS's have lost some elements and, consequently, the form of the possible AS's is less restrictive.

As has been shown, the sequence of phase transitions in this compound series are well described by adding an extra dimension. At any stage, the experimental space groups for each (rational) composition can be easily obtained from the common superspace group (Table 5 at high temperatures and Table 7 for the tilted and incommensurate phases). The analysis of the symmetry and the relationship between the symmetries of all the members of the compound series is simpler in the superspace framework than in the standard crystallographic description (compare with the analysis performed by Levin & Bendersky, 1999).

4. Comparison with experimental results

Structure determination of the $[Sr(Ti, Nb)O]_{(1-\gamma)}O_2$ compound series at high temperatures within the superspace framework reduces to the determination of the displacive modulations of Table 3. These displacive modulations are, in principle, and very often, in practice, found to be independent of composition. The superspace symmetry is common to the whole family (or compound series) with the only role of composition being to alter the value of γ associated with the modulation wavevector along **b**. At intermediate temperatures, the superspace group changes, but it again remains unique for the whole family (compound series). In this case, in addition to the displacive modulations, the average position of the O_2 atom in Table 8 must also be determined. In either case, once a final model has been obtained, the atomic positions for a given member of the compound series can be calculated by cutting the superspace construction perpendicular to x_4 with the appropriate composition-dependent size of the AS's and modulation wavevector magnitude γ. On the other hand, when the atomic positions of a given member of the compound series are known through a conventional crystallographic analysis, one can reconstruct the AS's by folding back the three-dimensional atomic positions onto the superspace unit cell. This is true for both sets of displacive modulations, the composition-dependent modulation parallel to the stacking direction as well as the incommensurate modulation along the **a** axis. As stressed above, there are some published structures which were determined using a conventional superstructure approach. It is worthwhile analyzing these particular cases within the superspace approach and to compare the results with the published data. A superspace description has already been used to describe the incom-

Table 8
General structural parameters in the superspace description of the high-temperature common structure with superspace group $C'mcb(0\gamma0)000(\gamma'00)0s0$.

a, *s* and no superscript represent antisymmetric, symmetric and arbitrary functions, respectively. Even (odd) superscript indicates that only even (odd) terms are present in the Fourier expansion series.

Element	x_1	x_2	x_3	x_4	x_5	Width of the AS	Point symmetry	Displacive modulation
Sr	0	0	0	0	0	$(1-\gamma)/2$	$2/m11$	$[x_1^{a,\mathrm{even}}(x_5), x_2^{a}(x_4)+x_2^{a,\mathrm{odd}}(x_5), x_3^{a}(x_4)+x_3^{a,\mathrm{odd}}(x_5)]$
Nb/Ti	$\frac{1}{2}$	0	$\frac{1}{2}$	0	0	$(1-\gamma)/2$	$2/m11$	$[x_1^{a,\mathrm{even}}(x_5), x_2^{a}(x_4)+x_2^{a,\mathrm{odd}}(x_5), x_3^{a}(x_4)+x_3^{a,\mathrm{odd}}(x_5)]$
O_1	0	0	$\frac{1}{2}$	0	0	$(1-\gamma)/2$	$2/m11$	$[x_1^{a,\mathrm{even}}(x_5), x_2^{a}(x_4)+x_2^{a,\mathrm{odd}}(x_5), x_3^{a}(x_4)+x_3^{a,\mathrm{odd}}(x_5)]$
O_2	$\frac{1}{2}$	y	z	0	0	$\frac{1}{2}$	$m11$	$[x_1^{a,\mathrm{even}}(x_5)+x_1^{s,\mathrm{odd}}(x_5), x_2(x_4)+x_2^{a,\mathrm{odd}}(x_5)+x_2^{s,\mathrm{even}}(x_5), x_3(x_4)+x_3^{a,\mathrm{odd}}(x_5)+x_3^{s,\mathrm{even}}(x_5)]$

mensurate modulation along the **a** axis (Yamamoto, 1982; Tanaka *et al.*, 1985; Nanot *et al.*, 1986; Grebille & Berar, 1987; Levin *et al.*, 2000), so we are primarily interested in the reconstruction of the composition-dependent displacive modulations. As the magnitude of the composition-dependent modulation wavevector is rational for all the refined structures, the number of distinct positions to translate into the superspace unit cell is finite and corresponds to a discrete set of points on the AS's. Obviously, the larger the number of independent atomic positions determined in the refined structures (the larger the denominator of the magnitude of the modulation wavevector $\gamma = r/s$), the more dense will be the discrete set of points which outline the AS. In the ideal limiting case of an incommensurate value of γ, the number of points on the AS is infinite and they trace out the corresponding AS as a dense set of points. The way to fold back refined three-dimensional atomic positions into superspace is straightforward and has been described in Elcoro *et al.* (2000).

Figs. 5(*a*) and (*b*) show an $x_2 - x_4$ projection of just such a superspace reconstruction for the tilted phase of the $Sr_2Nb_2O_7$ ($n = 4$) and $Sr_5Nb_5O_{17}$ ($n = 5$) compounds from Ishizawa *et al.* (1975) and Abrahams *et al.* (1998), respectively. In both figures, Sr, Nb and O atoms are represented by large, intermediate and small circles, respectively, and the meaning of the colors is the same as in Figs. 2 and 3. Four unit cells have been included to show the first neighboring coordinations and the complete AS's. The sets of atomic positions translated into the superspace unit cell are clearly ordered according to the general model proposed above. There are four different sets of AS's for both Sr and Nb atoms corresponding to the four types of layers, M, N, M′ and N′. The O atoms, however, are ordered into six different AS's representing the M, N, M′, N′, O and O′ layers. There are some important differences with respect to the ideal layer model picture depicted in Fig. 3. Firstly, the AS's corresponding to the O and O′ layers have different y coordinates so they appear split in the $y - x_4$ projection. This situation is different to what happens at high temperature, where the extra symmetry elements of the point group of the AS's representing the O layers force them to overlap. This splitting is due to the tilt around the **a** axis which occurs below the phase transition. According to Levin & Bendersky (1999) and Levin *et al.* (2000) neighboring layers of octahedra along the **b** direction (see Figs. 1*a* and *b*) rotate in antiphase around the **a** axis so that the two O atoms in an O or O′ layer move in the (y, z) plane. The two O atoms in the same layer move in opposite directions along the **b** axis. The same occurs along the **c** direction, but this component of the displacive modulation is not shown in the projection of Fig. 5.

Another important feature is the rather small deviation of the AS's representing O atoms from a vertical line. They are tilted slightly and the angle with respect to a vertical line is approximately the same for all these AS's. In physical space this means that a single layer of octahedra perpendicular to the stacking direction shifts as a whole along the **b** axis towards the closest vacancy layer. Displacements along **b** of consecutive layers are different. The closer the vacancy layer, the greater the shift, although this displacement is in all cases very small. By contrast, the amount of tilt of the AS's representing the Nb atoms (the intermediate circles in Figs. 5*a* and *b*) is noticeablely larger than the tilt of the AS's of the O atoms. In physical space, these cations are located inside octahedra and their mobility is very limited. The greater shift along **b** of their positions, however, means that they tend to get closer to the vacancy layer to compensate for the lack of positive charge. Finally, the AS's representing the Sr atoms (the big circles in Figs. 5*a* and *b*) are clearly divided into three pieces. The center of the AS has a small tilt with respect to the vertical line similar to the tilt of the AS representing the Nb atoms. These atoms correspond to the layers most distant from the vacancy layers and they try to follow the shift of the octahedra in the same layer. The outermost points on both sides of these AS's, however, are clearly separated from their centers. These atoms are the closest Sr atoms to the vacancy layers and they clearly shift from their ideal positions in a layer towards the vacancy layer to compensate for the local lack of positive charge. Their static displacements are much larger than the corresponding shifts of the Nb atoms within the same layer. The mobility of the Nb atoms is clearly restricted by the need to remain inside their local octahedron. In both Figs. 5(*a*) and (*b*), the displacement of the Sr atoms at the limits of the AS's along the y direction are approximately the same. Their projections fall between the two projections of the O atoms of the next layer (O or O′ green layers). Both figures support the idea that the structure in superspace (the content of the unit cell) is basically independent of composition. This experimental evidence has very important implications from the practical point of view. Once atomic positions have been obtained for a particular member of the compound series, and after the construction of a superspace model by folding these coordinates back into the superspace unit cell, it is possible to determine the atomic positions for another member of the compound series merely by changing the sizes of the AS's and the associated modulation wavevector

magnitude, both determined by the particular composition. Even more usefully, it should be possible to use diffraction data to determine directly the unknown structural parameters in the superspace description (see Table 8). Obviously, it would be advantageous to use diffraction data from a commensurate phase with a long period (large s in $\gamma = r/s$) to reduce the number of superpositions of reflections in reciprocal space or even from an incommensurate composition where no superpositions occur at all (providing of course that a single crystal of this type can be grown). The compound with the largest supercell refined up to now is that corresponding to Fig. 5(*b*) (the $n = 5$ member of the compound series). As Table 1 shows, however, there is another isomorphous phase corresponding to an $n = 6$ case, $(Nd_4Ca_2)Ti_6O_{20}$, whose structure (Nanot *et al.*, 1986; Grebille & Berar, 1987) has been determined *via* a conventional refinement. From this refinement, the atomic positions and displacive modulations in superspace have been determined. It is interesting to compare the obtained results with Figs. 5(*a*) and (*b*) to check whether the resulting AS's differ from the outlined AS's in these figures. Fig. 6 shows the result of folding back into the superspace unit cell the average atomic positions obtained by Grebille & Berar (1987). The results confirm our previous statement, *i.e.* the superspace model is practically independent of composition.

5. Conclusions

It has been shown that the $Sr_n(Nb, Ti)_nO_{3n+2}$ compound series can be uniquely described as modulated structures with a continuous variable, composition-dependent primary modulation wavevector. This analysis is valid even for non-rational compositions. The use of a superspace framework allows a unique structural model to be developed which is common to the whole family. The set of phase transitions with temperature of each of the members of this compound series can also be described in superspace *via* a change of the symmetry of the common superspace group. When the real structures are incommensurately modulated, the superspace analysis must be performed in five dimensions. The compositional modulations corresponding to the ideal layer stacking sequence for any particular composition are simple occupational crenel functions with a composition-dependent width. The displacive relaxations away from this ideal layer picture can be depicted by means of displacive modulations with an approximate sawtooth form, whose symmetry is determined by the average position of the AS.

The superspace framework has already been proved to be an efficient and unifying tool for the description of several intergrowth polytypoids (Evain *et al.*, 1998; Perez-Mato *et al.*, 1999; Elcoro *et al.*, 2000). In essence, the relevant superspace construction is a clever means to describe and store the atomic positions of commensurate structures having rather large conventional three-dimensional unit cells. The only fundamental requirement is that the atoms within this conventional unit cell should exhibit an approximate average periodicity of a rather smaller length scale, while the deviations from this average reference structure should be able to be described by only a relatively few parameters. In these homologous compound series, a smaller average periodicity is an essential intrinsic property resulting from their layered configuration. The actual layer stacking sequence taking place in each compound constitutes the primary modulation with respect to the average interlayer distance. This fundamental occupational modulation is described by '0/1' digital modulation functions which define the atomic domains or 'atomic surfaces' (AS's) in superspace and indicate which particular atomic position/layer occurs along the layer sequence. Structure determination then reduces to the determination of the displacive atomic modulations (whose symmetry is known) associated with the AS's. If the different types of layers are distributed along the layer sequence in a rather homogeneous way, maximizing for any particular composition somehow the distance between layers of the same type, the superspace description is bound to be quite simple. It is indeed rather independent of composition and the atomic positions are described by a few AS's.

The point which makes the superspace description specially powerful, however, is the fact that the superspace symmetry is unique and common to the whole compound series, while the conventional space group for any particular member or composition can be predicted by simple rules from this single superspace group. We cannot bring any rigorous theoretical argument demonstrating the composition invariance of the superspace group; it is an empirical fact, which is anew confirmed in this work for the compound series studied above. We have even been able to show that the same rule works for the symmetry changes taking place at temperature-driven phase transitions. Furthermore, the different four-dimensional superspace symmetries of the incommensurate phases observed in these compounds can be derived from a unique five-dimensional superspace group.

A further important empirical observation to be stressed is the fact that the refined atomic positions in all structures determined to date (by conventional crystallographic analysis) give rise to smoothly varying and essentially composition-independent displacive modulation functions (*cf.* Figs. 5 and 6) in superspace. Thus, polytypoids with long period sequences, and therefore large unit cells along the layer stacking direction, can be analyzed under this approach with not much greater difficulty than the shorter members of the series. By contrast, within a conventional crystallographic approach the number of free atomic parameters increases drastically with the size of the conventional unit cell. The superspace description keeps the number of structural parameters essentially unchanged, regardless of composition as long as the modulation functions remain smooth and describable by only a few parameters.

This work has been supported by the DGESIC (Project No. PB98-0244) and the UPV (Project No. 063.310-G19/98). We thank Professor Jacques Darriet for valuable comments. RLW thanks the support of Iberdrola as 'Profesor Visitante' at the Universidad del Pais Vasco, Bilbao.

References

Abrahams, S. C., Schmalle, H. W., Williams, T., Reller, T., Lichtenberg, F., Widmer, D., Bednorz, J. G., Spreiter, R., Bosshard, C. & Guenter, P. (1998). *Acta Cryst.* B**54**, 399–416.

Aurivillius, B. (1949). *Ark. Kemi*, **1**, 463–480.

Aurivillius, B. (1950). *Ark. Kemi*, **2**, 519–527.

Bak, P. (1985). *Phys. Rev. B*, **32**, 5764–5772.

Bak, P. (1986). *Scr. Metall.* **20**, 1199–1204.

Drews, A. R., Wong-Ng, W., Roth, R. S. & Vanderah, T. A. (1996). *Mater. Res. Bull. B*, **31**, 153–162.

Elcoro, L., Perez-Mato, J. M. & Withers, R. (2000). *Z. Kristallogr.* **215**, 727–739.

Evain, M., Boucher, F., Gourdon, O., Petricek, V., Dusek, M. & Bezdicka, P. (1998). *Chem. Mater.* **10**, 3068–3076.

Gourdon, O., Petricek, V. & Evain, M. (2000). *Acta Cryst.* B**56**, 409–418.

Grebille, D. & Berar, J. F. (1987). *Mater. Res. Bull.* **22**, 253–260.

Ishizawa, N., Marumo, F., Kawamura, T. & Kimura, M. (1975). *Acta Cryst.* B**31**, 1912–1915.

Janner, A. & Janssen, T. (1980). *Acta Cryst.* A**36**, 408–415.

Janssen, T., Janner, A., Looijenga-Vos, A. & de Wolf, P. M. (1992). *Tables for Crystallography*, edited by A. J. C. Wilson, p. 797. Dordrecht: Kluwer Academic Publishers.

Krishna, P. (1983). *Crystal Growth and Characterization of Polytype Structures.* Oxford: Pergamon Press.

Levin, I. & Bendersky, L. A. (1999). *Acta Cryst.* B**55**, 853–866.

Levin, I., Bendersky, L. A. & Vanderah, T. A. (2000). *Philos. Mag. A*, **80**, 411–445.

Levin, I., Bendersky, L. A., Vanderah, T. A., Roth, R. S. & Stafsudd, O. M. (1998). *Mater. Res. Bull.* **33**, 501–517.

Nanot, M., Queyroux, F., Gilles, J. C. & Capponi, J. J. (1986). *J. Solid State Chem.* **61**, 315–323.

Perez-Mato, J. M. (1992). *Methods of Structural Analysis of Modulated Structures and Quasicrystals*, edited by J. M. Perez-Mato, F. J. Zuniga and G. Madariaga, p. 117. Singapore: World Scientific.

Perez-Mato, J. M., Madariaga, G., Zuniga, F. J. & Garcia-Arribas, A. (1987). *Acta Cryst.* A**43**, 216–226.

Perez-Mato, J. M., Zakhour-Nakhl, M., Weill, F. & Darriet, J. (1999). *J. Mater. Chem.* **9**, 2795–2808.

Rao, C. N. R. & Rao, K. J. (1978). *Phase Transitions in Solids.* New York: McGraw-Hill.

Ruddlesden, S. N. & Popper, P. (1958). *Acta Cryst.* **11**, 54–55.

Tanaka, M., Sekii, H. & Ohi, K. (1985). *Jpn. J. Appl. Phys.* **24**, 814–816.

Van Tendeloo, G., Amelinckx, S., Darriet, B., Bontchev, R., Darriet, J. & Weill, F. (1994). *J. Solid State Chem.* **108**, 314–335.

Verma, A. R. & Trigunayat, G. C. (1974). *Solid State Chemistry*, edited by C. N. R. Rao. New York: Marcel Dekker.

Withers, R. L., Schmid, S. & Thompson, J. G. (1998). *Prog. Solid State Chem.* **26**, 1–96.

Yamamoto, N. (1982). *Acta Cryst.* A**38**, 780–789.